ECCOMAS Congress 2016
VII European Congress on Computational Methods in Applied Sciences and Engineering
M. Papadrakakis, V. Papadopoulos, G. Stefanou, V. Plevris (eds.)
Crete Island, Greece, 5–10 June 2016

AN EXACT SHEAR STRAIN APPROACH FOR RC FRAME ELEMENTS WITH AXIAL-SHEAR INTERACTION

Alexander Kagermanov[1], **Paola Ceresa**[2]

[1] UME School, Institute for Advanced Studies (IUSS)
Piazza della Vittoria, 15, 27100, Pavia, Italy
alexander.kagermanov@umeschool.it

[2] Institute for Advanced Studies (IUSS)
Piazza della Vittoria, 15, 27100, Pavia, Italy
paola.ceresa@iusspavia.it

Keywords: reinforced concrete, finite element analysis, frame elements, axial-shear interaction.

Abstract. *A fiber-section frame element for nonlinear analysis of two-dimensional, shear-critical reinforced concrete structures is developed. The element incorporates a new sectional algorithm for the computation of an exact shear strain profile and corresponding shear stress distribution. Longitudinal axial strains are evaluated based on the plane section assumption, while transverse strains are determined from equilibrium in the vertical direction, following classical beam assumptions. Axial-shear interaction at the fiber level is based on a smeared-crack, orthotropic constitutive model, which uses equivalent uniaxial material models for concrete and steel in the fixed-crack and reinforcement directions, respectively. Shear strain components at the crack, arising from deviations between principal and crack directions, are related to shear stresses by means of a shear stiffness term that fully satisfies compatibility and equilibrium conditions. The procedure was implemented into a force-based fiber element and applied to monotonic and cyclic analysis of shear-critical reinforced concrete structures. Validation examples include a number of experiments on lightly reinforced beams, shear-critical frames and columns.*

1 INTRODUCTION

Extensive experimental and analytical effort has been devoted to investigate the response of RC members under combined axial and shear stresses in the last 50 years. This allowed developing refined finite element models capable of predicting the global force-displacement response up to collapse, as well as local response parameters such as strains, crack widths and crack patterns. However, their general application to framed structures results cumbersome and time consuming, hence substantial effort is being addressed towards improving existing frame elements, usually based on the plane section assumption and uniaxial constitutive laws, in order to account for multi-axial loading conditions while keeping an efficient and simple formulation.

It can be said that a promising, fiber-based frame element for axial-shear interaction requires (i) an accurate multi-axial constitutive model and (ii) plausible section and beam kinematic assumptions. Extensive literature can be found concerning each of these topics. For instance, [1] introduced axial-shear interaction at the fiber level based on a dual-section analysis, whereby shear stresses over the section were calculated from the difference between axial stresses at two consecutive sections separated h/6 (h: depth of the member). [2] suggested a local procedure such that shear stresses were obtained from longitudinal gradients of deformations at a given section. Both authors used two-dimensional constitutive models, namely the Modified Compression Field Theory (MCFT), assuming that plane sections remain plane.

Several authors used Bernoulli and Timoshenko beam theories in both displacement- and force-based frame elements with axial-shear interaction [3]. The Bernoulli beam theory does not directly account for shear deformations, hence shear effects were usually introduced with an equivalent truss model, resulting only in partial coupling with axial forces and bending moments [4,5,6]. The Timoshenko beam theory provides a kinematic link between shear strains and transverse displacements of the beam axis. Hence, multi-axial constitutive models can be used at each individual fiber resulting in full axial-shear coupling [7, 8, 9, 10, 11, 12, 13]. However, the theory predicts a constant shear strain profile over the section, thus violating inter-fiber equilibrium. More recently, several higher-order theories were proposed dealing with the latter shortcomings [14, 15, 16, 17, 18]. Their application to nonlinear analysis of RC members is still in development. Moreover, their practical implementation for inelastic dynamic analysis needs further research due to complexities associated with their formulation and high computational demands.

The present work explores the possibility of an exact shear strain profile at the section level, while maintaining the plane section assumption for longitudinal strains. The rationale behind this approach is that [2], among others, demonstrated that axial-shear interaction in beams and columns can be relatively well captured assuming plane sections remain plane, whereas refined kinematic beam theories have not yet been fully verified. The exact shear strain profile is obtained from an averaged form of inter-fiber equilibrium over the section, using linear interpolation functions. The formulation was implemented into a force-based, fiber-element with smeared-crack, fixed-crack cyclic constitutive models. Verification examples on shear critical beams, frames and columns are provided at the end.

2 BEAM KINEMATICS

The Timoshenko beam theory is adopted to define the element kinematics. The total displacement of a given section point with coordinates (x, y) is given as:

$$u(x, y) = u_o(x) - \theta_z(x)y \tag{1}$$

$$v(x, y) = v_o(x) \tag{2}$$

where u_o is the horizontal displacement, θ_z the section rotation and v_o the vertical displacement of the beam axis, x the longitudinal coordinate along the beam axis, and y the vertical coordinate. Assuming small strain-displacement compatibility, fiber strains are defined from the linear Green-Lagrange strain tensor as:

$$\varepsilon_x = \frac{\partial u}{\partial x} = \frac{\partial u_o(x)}{\partial x} - \frac{\partial \theta_z(x)}{\partial x} y = \varepsilon_o - \chi_z y \tag{3}$$

$$\varepsilon_y = \frac{\partial v}{\partial y} = 0 \tag{4}$$

$$\gamma_{xy} = \frac{\partial v}{\partial x} - \frac{\partial u}{\partial y} = \frac{\partial v_o(x)}{\partial x} - \theta_z(x) = \gamma_{oy} \tag{5}$$

where ε_x is the axial strain, ε_y the transverse strain and γ_{xy} the shear strain acting on a section layer with coordinate y. ε_o is the section axial strain, χ_z the section curvature and γ_{oy} section shear deformation. The relationship between strains and section deformations can be expressed as:

$$\begin{pmatrix} \varepsilon_x \\ \gamma_{xy} \end{pmatrix} = \begin{bmatrix} 1 & -y & 0 \\ 0 & 0 & 1 \end{bmatrix} \begin{pmatrix} \varepsilon_o \\ \chi_z \\ \gamma_{oy} \end{pmatrix} \tag{6}$$

$$\boldsymbol{\varepsilon} = \mathbf{B}\mathbf{e} \tag{7}$$

Section forces are obtained from direct integration of stress distributions over the section:

$$\mathbf{S} = \int_A \mathbf{B}^T \boldsymbol{\sigma} dA \tag{8}$$

where $\mathbf{S}=[N,M,V]^T$ and $\boldsymbol{\sigma}=[\sigma_x, \tau_{xy}]^T$ are the vector of section forces and stresses, respectively. The tangent stiffness matrix of the section is obtained taking variation of section forces with respect to section deformations:

$$\mathbf{K}_s = \frac{\partial \mathbf{S}}{\partial \mathbf{e}} = \frac{\partial}{\partial \mathbf{e}} \int_A \mathbf{B}^T \boldsymbol{\sigma} dA = \int_A \mathbf{B}^T \frac{\partial \boldsymbol{\sigma}}{\partial \boldsymbol{\varepsilon}} \frac{\partial \boldsymbol{\varepsilon}}{\partial \mathbf{e}} dA = \int_A \mathbf{B}^T \frac{\partial \boldsymbol{\sigma}}{\partial \boldsymbol{\varepsilon}} \mathbf{B} dA = \int_A \mathbf{B}^T \bar{D} \mathbf{B} dA \tag{9}$$

where $\bar{D}$ is the condensed, 2×2 material stiffness matrix, given as:

$$\begin{pmatrix} \partial\sigma_x \\ \partial\tau_{xy} \end{pmatrix} = \begin{bmatrix} \bar{D}_{11} & \bar{D}_{12} \\ \bar{D}_{21} & \bar{D}_{22} \end{bmatrix} \begin{pmatrix} \partial\varepsilon_x \\ \partial\gamma_{xy} \end{pmatrix} \tag{10}$$

Condensation is carried out upon neglecting the effect of clamping forces, that is, assuming that $\sigma_y=0$, which is a reasonable approximation in regions away from local disturbance, such as supports and points of load application. In this case, the increment of transverse strains is given as:

$$\partial\varepsilon_y = \frac{(-D_{21}\partial\varepsilon_x - D_{23}\partial\gamma_{xy})}{D_{22}} \tag{11}$$

where D_{21}, D_{22} and D_{23} are coefficients of the 3×3 material stiffness matrix relating ($\partial\sigma_x$, $\partial\sigma_y$, $\partial\tau_{xy}$) and ($\partial\varepsilon_x$, $\partial\varepsilon_y$, $\partial\gamma_{xy}$), obtained from the two-dimensional constitutive model presented in the next sections.

3 SHEAR STRAIN PROFILE

The section model is based on the evaluation of an exact shear strain profile using the inter-fiber equilibrium equation. This can be derived from internal beam equilibrium in the longitudinal direction:

$$-\sigma_x dy - \tau_{xy} dx + \sigma_x dy + \frac{\partial \sigma_x}{\partial x} dx dy + \tau_{xy} dx + \frac{\partial \tau_{xy}}{\partial y} dy dx = 0 \tag{12}$$

$$\frac{\partial \sigma_x}{\partial x} + \frac{\partial \tau_{xy}}{\partial y} = 0 \tag{13}$$

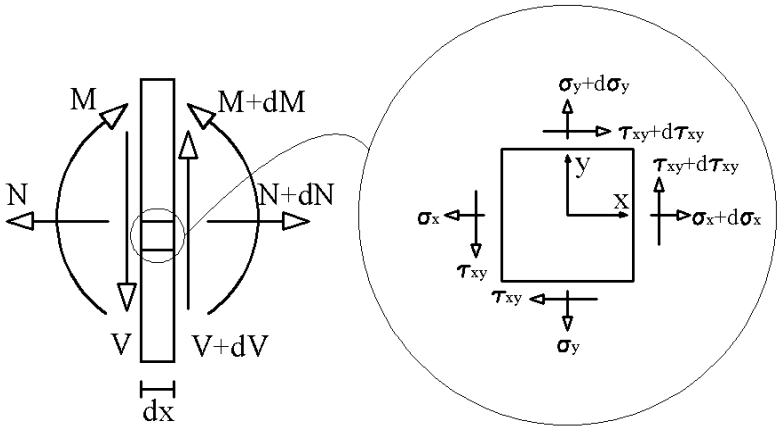

Figure 1: Internal equilibrium in a cross-section plane stress element.

Using the constitutive relationship in equation (10) in conjunction with equation (13) yields:

$$\overline{D}_{11} \frac{\partial \varepsilon_x}{\partial x} + \overline{D}_{12} \frac{\partial \gamma_{xy}}{\partial x} + \overline{D}_{21} \frac{\partial \varepsilon_x}{\partial y} + \overline{D}_{22} \frac{\partial \gamma_{xy}}{\partial y} = 0 \tag{14}$$

The first two terms in (14) contain strain derivatives in the longitudinal direction. These can be obtained from the derivative of section forces and compatibility between fiber and section strains:

$$\frac{d\mathbf{e}}{dx} = \mathbf{K}_s^{-1} \frac{d\mathbf{S}}{dx} \tag{15}$$

$$\frac{\partial \boldsymbol{\varepsilon}}{\partial x} = \mathbf{B} \frac{d\mathbf{e}}{dx} \tag{16}$$

where $d\mathbf{S}/dx=[0,-V,0]^T$ for an element under constant axial load and shear, and linear variation of bending moments. The term $\partial\varepsilon_x/\partial y$ in (14) is equal to $-\chi_z$ from (3), and $\partial\gamma_{xy}/\partial y$ is obtained from interpolation of γ_{xy} using linear shape functions such that:

$$\gamma_{xy} = \mathbf{N}\boldsymbol{\gamma} = N_i \gamma_i + N_j \gamma_j \tag{17}$$

$$\mathbf{N} = \begin{pmatrix} N_i & N_j \end{pmatrix} = \left(\frac{y_j - y}{y_j - y_i} \quad \frac{y - y_i}{y_j - y_i} \right) \tag{18}$$

where γ_i, γ_j are nodal values of shear strain at the ends of the l^{th} layer, and y_i and y_j the corresponding coordinates (Figure 2).

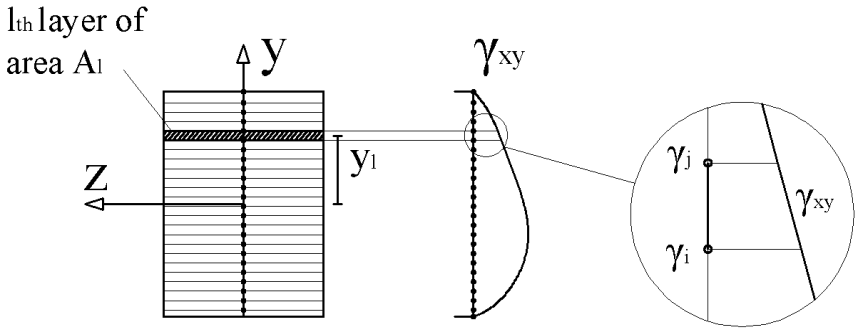

Figure 2: Interpolation of the shear strain profile.

Inter-fiber equilibrium in equation (13) is invoked in a weighted average form over the cross section, using as a weighting function the derivative of the shear strain, $\partial\gamma_{xy}/\partial y$. Upon accounting for the contribution of each individual layer, this is expressed in the following functional form:

$$\mathop{\mathbf{A}}_{l=1}^{nl} \int_{Al} \delta\gamma'^{T}_{xy} \left(\frac{\partial \sigma_x}{\partial x} + \frac{\partial \tau_{xy}}{\partial y} \right) dA = 0 \tag{19}$$

where A is the assemblage operator over the section layers, nl number of layers, A_l the area of the l^{th} layer, and $\delta\gamma_{xy}'$ the virtual derivative of the shear strain. Substituting equations (14) and (17) into (19) yields:

$$\mathop{\mathbf{A}}_{l=1}^{nl} \int_{Al} \delta\boldsymbol{\gamma}^{T} \left(\mathbf{N}'^{T} C + \mathbf{N}'^{T} \overline{D}_{22} \mathbf{N}' \boldsymbol{\gamma} \right) dA = 0 \tag{20}$$

$$C = \overline{D}_{11} \frac{\partial \varepsilon_x}{\partial x} + \overline{D}_{12} \frac{\partial \gamma_{xy}}{\partial x} + \overline{D}_{21} \frac{\partial \varepsilon_x}{\partial y} \tag{21}$$

Since $\delta\boldsymbol{\gamma}$, containing the virtual nodal shear strains, is non-zero, the vector of nodal shear strains $\boldsymbol{\gamma}$ can be obtained from solving:

$$\boldsymbol{\gamma} = \mathbf{k}^{-1}\mathbf{f} \tag{22}$$

where:

$$\mathbf{k} = \mathop{\mathbf{A}}_{l=1}^{nl} \int_{Al} \mathbf{N}'^{T} \overline{D}_{22} \mathbf{N}' dA \tag{23}$$

$$\mathbf{f} = -\mathop{\mathbf{A}}_{l=1}^{nl} \int_{Al} \mathbf{N}'^{T} C dA \tag{24}$$

4 FINITE ELEMENT IMPLEMENTATION

4.1 Force-based formulation

The proposed section model was implemented into a two-dimensional, force-based fiber element according to [19]. In this formulation, once the global displacements are known, an iterative state determination procedure is invoked at the element level in order to find the corresponding section strains at each integration point. Because section forces are known at the start of the state determination procedure, from the exact interpolation of element forces, and section deformations can be estimated using the current section flexibility matrix, all the ingredients for the calculation of the "exact" shear strain profile are available. Thus, the three total strain components (ε_x, ε_y, γ_{xy}) at each individual fiber are known. The corresponding stresses, (σ_x, σ_y, τ_{xy}), are obtained from the constitutive model and integrated to yield the section forces. In subsequent element iterations, the initial shear strain profile is corrected based on the unbalanced vector of section forces until satisfying section equilibrium. Further details on the numerical implementation are given elsewhere [20].

4.2 Constitutive model

The constitutive model is based on a smeared-crack, single fixed-crack membrane model [21]. For concrete, equivalent uniaxial constitutive relationships are applied in the fixed-crack directions (figure 3), while shear components arising from deviation between principle directions and crack directions are related through the secant shear stiffness term given as:

$$G = \frac{(\sigma_1 - \sigma_2)(\sin\Delta\theta_\sigma \cos\Delta\theta_\sigma)}{2(\varepsilon_1 - \varepsilon_2)(\sin\Delta\theta_\varepsilon \cos\Delta\theta_\varepsilon)} \tag{25}$$

where σ_1, σ_2, and ε_1, ε_2 are the principal stresses and strains, respectively, and $\Delta\theta_\sigma$, $\Delta\theta_\varepsilon$ the corresponding angles between principle and crack directions.

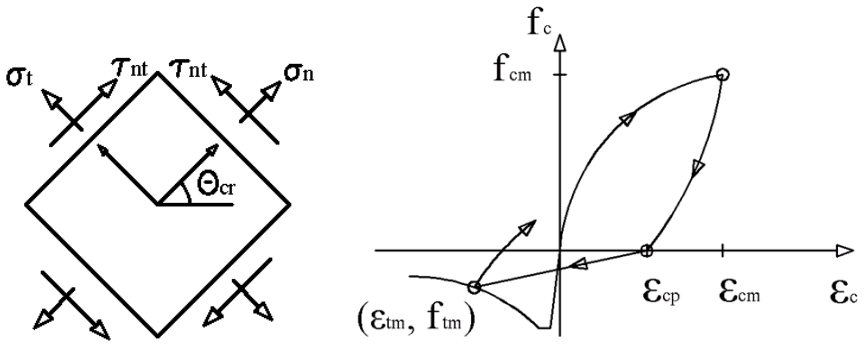

Figure 3: Fixed-crack reference system and cyclic constitutive model.

The cyclic response in tension is obtained from a physically-based approach, whereby tension stiffening, crack-opening and crack-closing branches are computed from average equilibrium on a cracked element of reinforced concrete (figure 4). Further details can be found in [21].

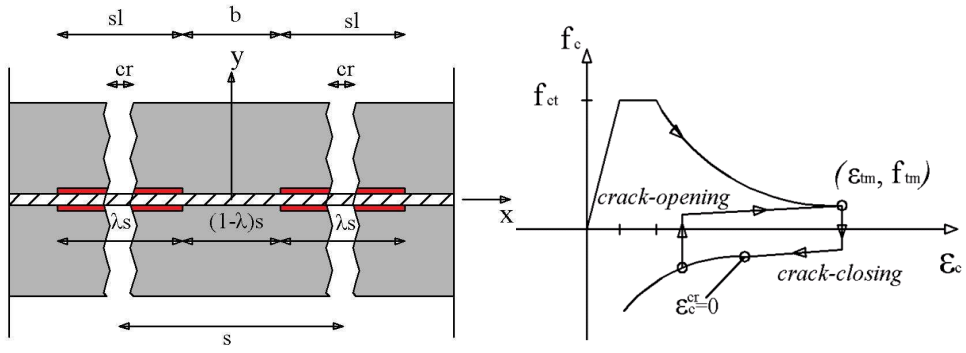

Figure 4: Cracked element of reinforced concrete and cyclic response in tension.

5 NUMERICAL VERIFICATION

5.1 Shear critical beams.

Beams OA1 and A1, tested by Bresler and Scordelis 1963 [22], were two simply supported beams with 305mm x 552mm rectangular cross sections and 3660mm clear span. Beam A1 presented 6.4mm diameter stirrups spaced at 210mm, whereas beam OA1 was unreinforced in shear and only presented bottom reinforcement (Table 2). Beam OA1 failed in diagonal-tension along the shear-critical crack with accompanying longitudinal splitting in the bottom flexural reinforcement. Beam A1 failed in shear-flexure, involving the formation of diagonal shear cracks and concrete crushing in the compression zone next to the loading plate [25].

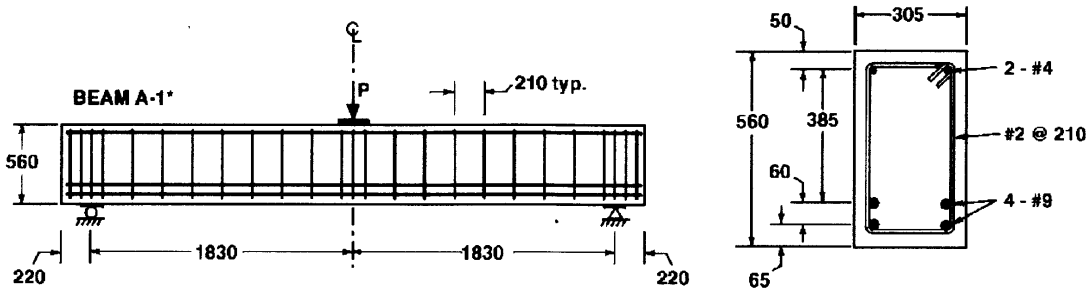

Figure 5: Beam test set up and cross section [22].

Beam	OA1	A1	Steel	Diameter(mm)	f_y(MPa)	f_u(MPa)	E_s(MPa)
Compressive strength(MPa)	22.6	24.1	Nº2	6.4	325	3660	190000
Peak Strain	0.0018	0.0018	Nº4	12.7	127	3660	201000
			Nº9	28.7	645	3660	218000

Table 1: Beam material properties.

Beam	Width(mm)	Height (mm)	Effective depth(mm)	Length(mm)	Span(mm)	Bottom Steel	Top Steel	Stirrups
OA1	310	556	461	4100	3660	4Nº9	-	-
A1	307	561	466	4100	3660	4Nº9	2Nº4	Nº2@210

Table 2: Beam geometric properties.

The beams were modeled with one single frame element with 5 integration points (IPs) (Gauss-Legendre integration rule), representing half of the beam due to symmetry conditions. The cross section was discretized into 21 layers of equal thickness. The influence of longitudinal reinforcement was smeared over the layers located within a distance of $7.5d_b$ (d_b: bar diameter) at both sides of the reinforcement. The analysis was performed under displacement control with 1mm displacement increments. Figure 6 compares the analytical and experimental responses. Also, results from FE analysis reported in [25], performed with 15×46 constant-strain, membrane finite elements based on a rotating-crack approach, are included.

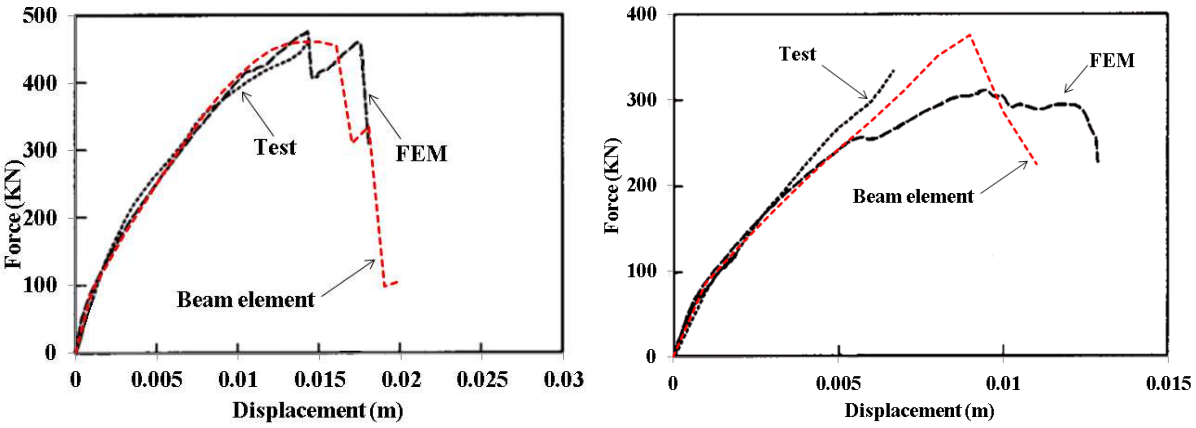

Figure 6: Force-displacement response of beams A1 (left) and OA1 (right) [25]

Figure 7 and figure 8 show calculated shear strains, shear stresses and normal concrete stresses over the depth of the section at the closest to the applied load IP, at three different displacement levels. It can be observed that the parabolic shear strain assumption approximately holds at early load stages, before significant crack-induced anisotropic behavior develops. In later stages, shear strains in the compression zone tend to decrease and concentrate in the lower portion of the web. Note that for beam A1 concrete crushing in the top compression zone occurs, suggesting that the beam ultimately failed in combined shear-compression mode, whereas for beam OA1 normal concrete stresses remain below the compressive strength. These results are consistent with the experimental observations, as previously described.

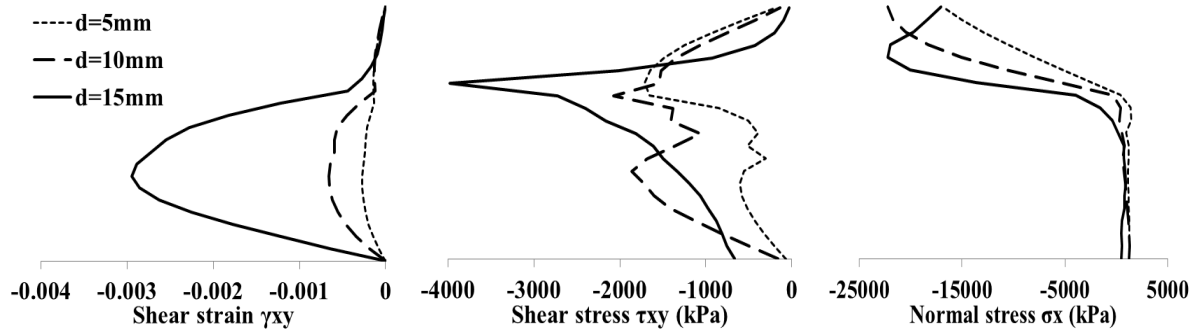

Figure 7: Shear strain, shear stress and normal concrete stress profiles for beam A1.

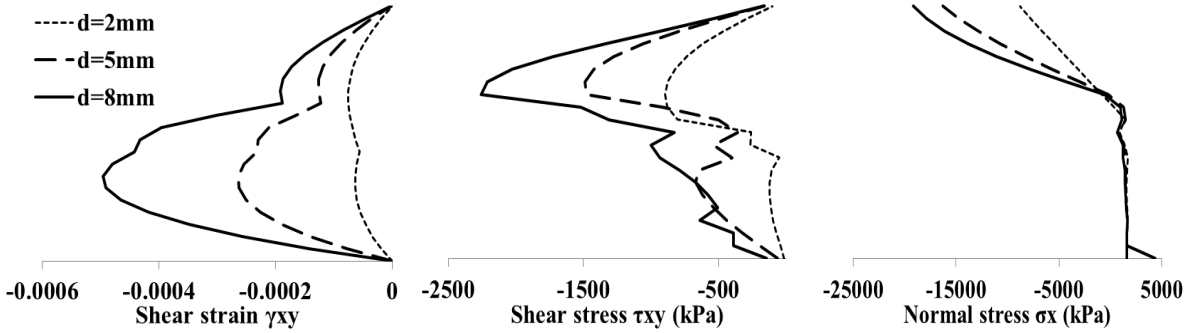

Figure 8: Shear strain, shear stress and normal concrete stress profiles for beam OA1.

5.2 Shear critical frame

The RC frame tested by Duong et al. 2007 [23] failed in brittle mode due to shear failure of the beams. It was a one-bay, two-story frame with an applied vertical load of 420 kN at the top of each column, subjected to an increasing lateral force at the second level (figure 9). Material properties for steel and concrete are summarized in table 3. The frame was pushed in one direction, until substantial diagonal cracking of the beams occurred, and then in the opposite direction until completing one full cycle.

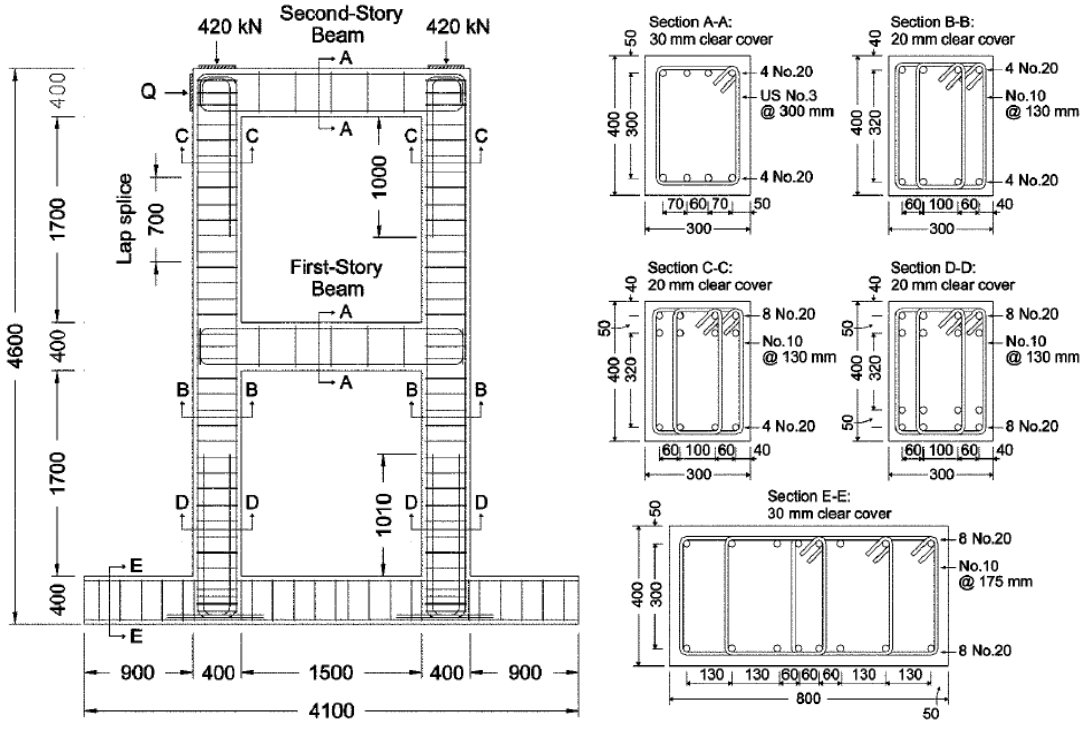

Figure 9: Geometric properties of the frame [23]

Concrete		
Compressive strength(MPa)	Peak Strain	Young Modulus(MPa)
42.9	0.0023	30058

Steel						
Bar Size	Diameter(mm)	Area(mm^2)	f_y(MPa)	f_u(MPa)	E_s(MPa)	ε_u‰
φ20	19.5	300	447	603	198400	130.8
φ 10	11.3	100	455	583	192400	129.9
US #3	11.3	71	506	615	210000	134.6

Table 3: Frame material properties.

Each column was modeled with two frame elements per story in order to consider the increase in longitudinal reinforcement ratios at the ends of the columns. One single element was used for each beam, being the number of integration points 5/element, for both beam and column elements. The cross section was discretized into 11 layers of equal thickness. Centerline dimensions were used to define the geometry of the frame, which was assumed rigidly fixed at the foundation level. No particular modeling of the joint flexibility was undertaken. Comparison between analytical and experimental lateral force-top displacement responses is shown in figure 10, for both monotonic and cyclic load cases. The monotonic analysis predicts an ultimate displacement of about 47mm, very close to the unloading point (45mm) at which substantial shear cracking of beams was observed during the test.

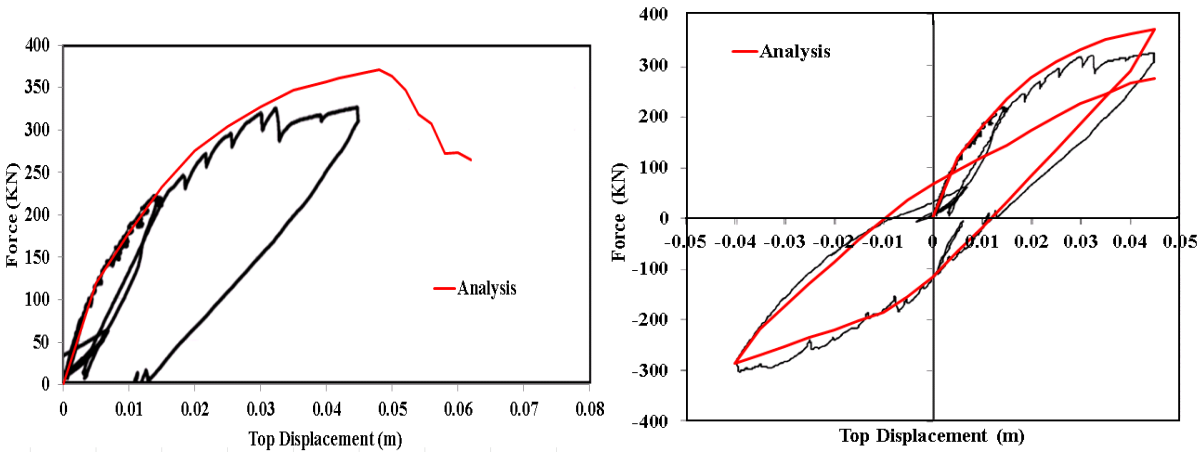

Figure 10: Force-displacement response for the monotonic (left) and cyclic (right) case.

The calculated shear strains, shear stresses and normal concrete stresses over the section are depicted in figure 11 for the first story beam, at the IP closest to the right column. Note again the reduction in shear strains in the compressive zone.

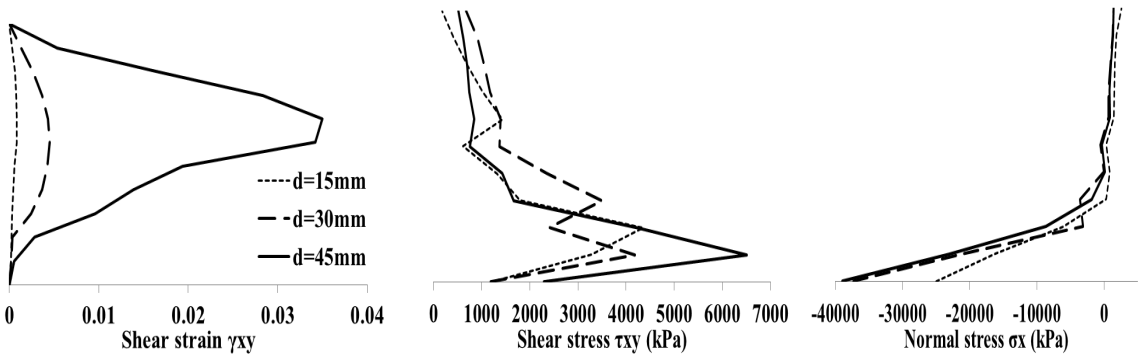

Figure 11: Shear strain, shear stress and normal concrete stress profiles for the 1st story beam.

5.3 RC bridge pier

The RC bridge pier R1 tested by Xiao et al. 1994 [24] had an aspect ratio of 4, 603mm x 406mm rectangular cross-section and 2398mm clear height (Figure 12). The pier was tested in double curvature, with the top and bottom rotations fixed, resulting in a shear span of 2. Longitudinal reinforcement consisted of 22, 20mm bars distributed around the perimeter of the section. Shear reinforcement consisted of 6.35mm rectangular hoops spaced at 127mm. A permanent axial load of 501kN was applied at the top of pier. The pier was subjected to increasing displacement increments at different levels of ductility.

Concrete		Bar Size	Diameter(mm)	f_y(MPa)	f_u(MPa)	ε_u‰
Compressive strength(MPa)	38	#6	19.5	317	453	110
Young Modulus(MPa)	30820	#2	6.35	361	483	110

Table 4: Bridge pier material properties.

The pier was modeled with one single element (5IPs) 2438mm long, fully fixed at the bottom and with the top node restrained against rotation. The section was discretized into 11 layers of equal thickness and the reinforcement distributed according to the layout. The top horizontal degree of freedom was subjected to increasing cyclic displacement. Experimental and analytical results are compared in Figure 12. An overestimation of the initial stiffness can be observed due to the fact that the specimen was pre-cracked under initial small-displacement excursions during the test. Good agreement is found in terms of strength, loading/unloading stiffness and permanent displacements. Results from monotonic analysis indicated imminent failure of the specimen at approximately 40mm top displacement.

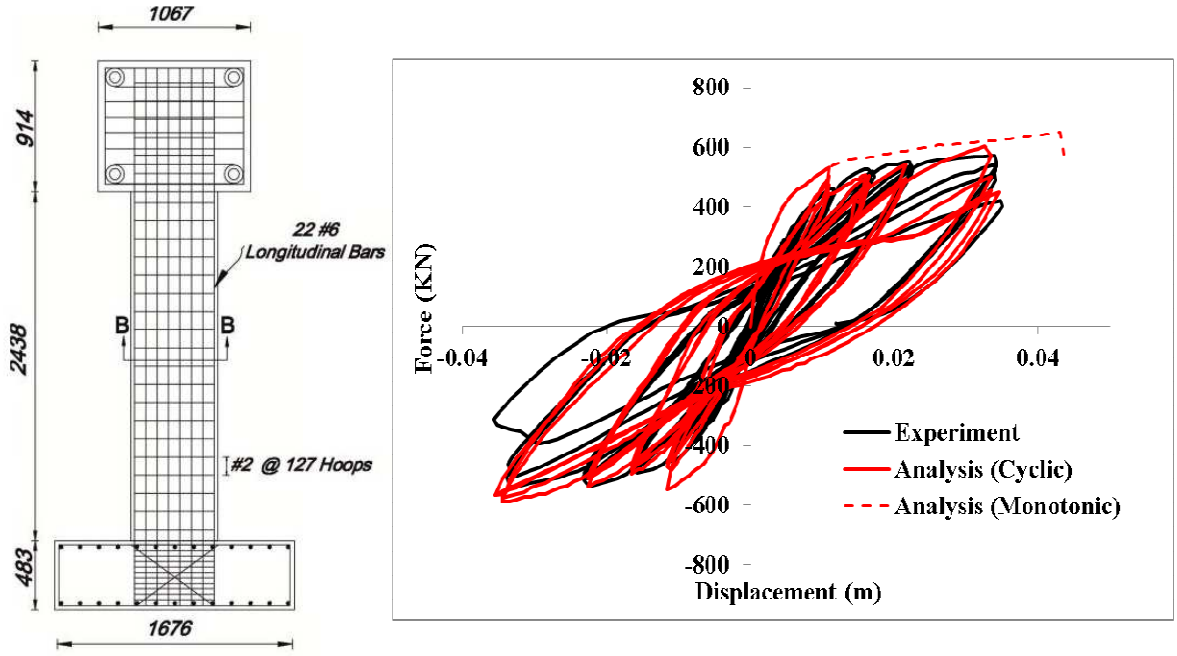

Figure 12: Bridge pier geometry and horizontal force-displacement response [24].

6 CONCLUSIONS

The proposed section model for the evaluation of an exact shear strain profile was satisfactorily implemented within a force-based, fiber-based frame element for monotonic and cyclic analysis of shear-critical RC structures.

Conceptually speaking, the element is superior to elements with fixed shear strain profiles, such as those with constant or parabolic patterns. However, the element kinematics still relies on the Timoshenko beam theory, i.e. plane section assumption and no section distorsion or warping, resulting in kinematic incompatibility between fiber deformations and element displacements.

A number of verification examples on shear-critical RC beams, frame and pier showed relatively good agreement in terms of post-cracked stiffness, shear strength and ultimate displacement capacity. Realistic stress and strain distributions over the section were obtained. However, further verification and comparison with experimental data is required.

REFERENCES

[1] F.J. Vecchio, M. P. Collins, Predicting the response of RC members subjected to shear using the Modified Compression Field Theory. *ACI Structural Journal,* **85**(3), 258-268, May-June 1988.

[2] E.C. Bentz, Section analysis of reinforced concrete members. *PhD Thesis,* Department of Civil Engineering, University of Toronto, 2000.

[3] P. Ceresa, L. Petrini, R. Pinho, Flexure-Shear Fiber Beam-Column Elements for Modeling Frame Structures Under Seismic Loading — State of the Art, *Journal of Earthquake Engineering,* **11**(1), 46–88, 2007.

[4] J. Guedes, P. Pegon, A. Pinto, A Fibre/Timoshenko Beam Element in CASTEM 2000, *Special Publication Nr. I.94.31* Applied Mechanics Unit, Safety Technology Institute, Commission of the European Communities, Joint Research Centre, Ispra Establishment, Italy, 1994.

[5] L. Martinelli, Modellazione di pile di ponti in C. A. a travata soggetti ad eccitazione sismica, *PhD Thesis*, Dipartimento di Ingegneria Strutturale, Politecnico di Milano, Milano, Italy, 1998.

[6] G. Ranzo, M. Petrangeli, A fibre finite beam element with section shear modelling for seismic analysis of RC structures, *Journal of Earthquake Engineering*, **2**, 443–473, 1998.

[7] M. Petrangeli, P. E. Pinto, V. Ciampi, Fibre element for cyclic bending and shear of RC structures. I: theory, *Journal of Engineering Mechanics*, **125**(9), 994-1001, 1999.

[8] M. Petrangeli, P. E. Pinto, V. Ciampi, Fibre element for cyclic bending and shear of RC structures. II: verification, *Journal of Engineering Mechanics*, **125**(9), 1002-1009, 1999.

[9] P. Ceresa, L. Petrini, R. Pinho, R. Sousa, A fibre flexure–shear model for seismic analysis of RC-framed structures, *Earthquake Engineering and Structural Dynamics*, **38**, 565-586, 2009.

[10] J.N. Gregori, P.M. Sosa, M.A.F. Prada, F.C. Filippou, 3D frame element for the analysis of reinforced and prestressed concrete structures subjected to shear and torsion loads, *Engineering Structures*, **29**(12), 3404-3419, 2007.

[11] S. Gühner, Performance Assessment of Shear-Critical RC Frames. *PhD Thesis,* Department of Civil Engineering, University of Toronto, 2008.

[12] T. R. S. Mullapudi, A. Ayoub, Analysis of Reinforced Concrete Columns Subjected to Combined Axial, Flexure, Shear, and Torsional Loads, *Journal of Structural Engineering*, **139**(4), April 1, 2013.

[13] J. Mazars, P. Kotronis, F. Ragueneau, G. Casaux, Using multifiber beams to account for shear and torsion Applications to concrete structural elements*, Computers Methods in Applied Mechanics and Engineering*, **195**(52), 7264–7281, 2006.

[14] J.M. Bairán, A.R. Marí, Shear-Bending-Torsion Interaction in Structural Concrete Members: A Nonlinear Coupled Sectional Approach. *Computational Methods in Engineering*, **14**,249-278, 2007.

[15] S. Mohr, J.M. Bairan, A.R. Mari, A frame element model for the analysis of reinforced concrete structures under shear and bending, *Engineering Structures*, **32**,3936-3954, 2010.

[16] J. Pacheco Almeida, Flexure-Shear Element for 3D Inelastic Analysis of Frames, *PhD Thesis*, ROSE School, Università degli Studi di Pavia, 2009.

[17] V. Le Corvec, Nonlinear 3d frame element with multi-axial coupling under consideration of local effects, *PhD Thesis*, Department of Civil and Environmental Engineering, UC Berkeley, 2012.

[18] A. Papachristidis, M. Fragiadakis, M. Papadrakakis, A 3D fibre beam-column element with shear modeling for the inelastic analysis of steel structures. Computational Mechanics 45, 553–572, 2010.

[19] E. Spacone, V. Ciampi, F.C. Filippou, Mixed formulation of nonlinear beam finite element. *Computer Structures* 58(1), 71–83, 1996.

[20] A. Kagermanov. An exact shear strain evaluation for two-dimensional RC frame elements. *PhD Thesis,* UME School, Institute for Advanced Studies, Pavia, Italy, 2016.

[21] A. Kagermanov. Physically-based cyclic tensile model for RC membrane elements. *Individual Study,* UME School, Institute for Advanced Studies, Pavia, Italy, 2015.

[22] B. Bresler, A.C. Scordelis, Shear strength of RC beams, ACI Journal Proceedings, **60**(1), 51-74, 1963.

[23] K.V. Duong, S.A Sheikh, F.J. Vecchio, Seismic Behaviour of Shear-Critical Reinforced Concrete Frame: Experimental Investigation. *ACI Structural Journal*, 104(3), May-June, 304-313, 2007.

[24] Y. Xiao, M. J. N. Priestley, F. Seible, Steel Jacket Retrofit for Enhancing Shear Strength of Rectangular Short Reinforced Concrete Columns. *Structural Systems Research Project*, Report No. SSRP 92/07, University of California, San Diego, June, 1993.

[25] F.J. Vecchio, W. Shim, Experimental and Analytical Reexamination of Classic Concrete Beam Tests, *Journal of Structural Engineering*, 130(3), March 1, 2004.